

## Article

# Analysing and Computing the Impact of Geometric Asymmetric Coils on Transformer Stray Losses

Ivan A. Hernandez-Robles <sup>1</sup>, Xiomara Gonzalez-Ramirez <sup>1,\*</sup>, Juan C. Olivares-Galvan <sup>2</sup>,  
Rafael Escarela-Perez <sup>2</sup> and Rodrigo Ocon-Valdez <sup>3</sup>

<sup>1</sup> Departamento Ingeniería Eléctrica, Universidad de Guanajuato, Guanajuato 36885, CP, Mexico; ia.hernandez@ugto.mx

<sup>2</sup> Departamento de Energía, Universidad Autónoma Metropolitana, Mexico City 02120, CP, Mexico; jolivares@azc.uam.mx (J.C.O.-G.)

<sup>3</sup> Ingeniería Eléctrica y Electrónica, Universidad Nacional Autónoma de Mexico, FES Aragón, Mexico City 57171, CP, Mexico; rodrigocon99@aragon.unam.mx

\* Correspondence: x.gonzalez@ugto.mx

**Abstract:** Designing and manufacturing transformers often involves variations in heights and thicknesses of windings. However, such geometric asymmetry introduces a significant impact on the magnitude of stray transformer losses. This study examines the effects of asymmetric coils on the generation of stray losses within core clamps and transformer tank walls. A model has been introduced to ascertain the dispersion magnetic field's value at a specific distance from the coil. The analysis extends to characterising the dispersion magnetic field reaching the tank walls by using electromagnetic simulation by a finite element method. It explores strategies to diminish stray losses, including the placement of magnetic shunts as protective shields for the tank walls. It delves into the efficacy of employing a transformer shell-type configuration to mitigate the magnetic dispersion field. The findings revealed that achieving greater symmetry in transformer coils can minimise stray losses. Specifically, the incorporation of magnetic shunts has the potential to reduce additional losses by 40%, while the adoption of a shell-type configuration alone can lead to a 14% reduction. This work provides valuable insights into optimising transformer designs, contributes a user-friendly tool for estimating additional tank losses, thereby enhancing the knowledge base for transformer manufacturers.

**Keywords:** electromagnetic simulation; geometric asymmetric coils; magnetic shunts; stray magnetic flux; transformers



**Citation:** Hernandez-Robles, I.A.; Gonzalez-Ramirez, X.; Olivares-Galvan, J.C.; Escarela-Perez, R.; Ocon-Valdez, R. Analysing and Computing the Impact of Geometric Asymmetric Coils on Transformer Stray Losses. *Appl. Syst. Innov.* **2024**, *7*, 26. <https://doi.org/10.3390/asi7020026>

Academic Editor: Emmanuel Karapidakis

Received: 8 February 2024

Revised: 7 March 2024

Accepted: 15 March 2024

Published: 25 March 2024



**Copyright:** © 2024 by the authors. Licensee MDPI, Basel, Switzerland. This article is an open access article distributed under the terms and conditions of the Creative Commons Attribution (CC BY) license (<https://creativecommons.org/licenses/by/4.0/>).

## 1. Introduction

It is now widely recognised that some of the dispersion magnetic field generates stray losses within the structural components of the transformer and its associated tank. It is also recognised that as transformer power increases, this stray flux can cause substantial losses, resulting in heating effects. Recent advances in research focuses on various aspects of stray losses within transformer tanks. These studies employ a variety of methodologies, including numerical techniques such as the finite element method, as well as analytical and experimental approaches [1–6]. In this work, stray magnetic field refers to the dispersion magnetic field that reaches the tank and core clamp, and that produces stray losses in them. Research has demonstrated that stray losses resulting from induced current by eddy currents on tanks and other structural elements of distribution transformers can amount more than 15% of the corresponding load losses [7]. In the transformer industry (especially in power transformers), this knowledge has led to adapting the transformer with magnetic shunts and other accessories to reduce load losses in their equipment. The challenge of identifying and mitigating parasitic losses in metallic components and transformer tanks is not a recent problem. It has been widely addressed in technical literature [8–11]. Some

transformer manufacturers continue to use the empirical analytical formulas from this literature or from their experience in their current practices. Calculating stray losses requires an understanding of the stray magnetic field. To address this problem, efficient methods have emerged to quickly and approximately estimate the equivalent leakage reluctance, in particular by using the Reluctance Network Modelling (RNM) method [12,13]. The adoption of numerical methods, such as the Finite Element Method (FEM), has greatly facilitated the evaluation of the stray magnetic field and its associated additional losses. These methods make the simulation of stray magnetic fields in two- and three-dimensional scenarios more accessible and less complex. However, it is imperative to note that the utilisation of such methods comes at the expense of high computational requirements during the transformer design stage. These considerations are essential to effectively reduce stray losses and prevent hot spots. Furthermore, the application of the Finite Element Method (FEM) has allowed us to examine the impact of additional factors, such as geomagnetically induced currents, that contribute to increased stray losses in the transformer tank [14]. Minimising stray losses in transformers represents an important competitive advantage in the industry. Consequently, there has been an increase in research dedicated to identifying the optimal location of magnetic shunts, with the objective of decreasing stray losses within the transformer tank [15,16]. The research is also focused on finding the optimal geometry of the magnetic shunt [17]. The orientation of the shunt also plays an important role in reducing losses, which is why works such as [18] clearly and conclusively confirm the effectiveness of orienting the shunt horizontally. In [19] non-magnetic stainless steel, an insert was utilized to reduce the stray losses in a significant way in 80% of the region of the Tertiary Voltage Bushings of the transformer. The effect of magnetic shunts on shell-type transformers' characteristics was recently analysed and determined. This helped in determining the magnetic flux density distributions, and the points with high values in the shell-type core and movable shunt sub-areas [20]. Despite the important technical literature on this topic, in the design stage there are still some technical doubts about how the stray magnetic field is affected when there are different widths and heights of the windings. In the design, it is common and very normal for the thicknesses of the windings to be different and the height of the high voltage winding to be similar to the height of the low voltage winding, but most of the time it is not possible to achieve this, so this work contributes to the analysis and quantification of the effect of these differences in dimensions in the windings on the stray magnetic flux that reaches the tank. Therefore, it helps to have an overview of its magnetic field density, which assists in controlling additional losses. In this work, the characterisation of the magnetic field that reaches the tank walls was added along with a quick-to-apply model to approximately estimate the stray magnetic field from the coil to the limits of the tank walls and the impact of reducing stray losses by placing magnetic shunts and using a shell-type configuration transformer. This work also considers three different materials (Mill Anneal Steel, Grain Oriented Silicon Steel and Amorphous Silicon Steel) for the shunts in order to analyse their effectiveness and cost. Therefore, the objective of this research is to serve as a valuable tool in the design and manufacturing processes of transformers. Therefore, this work has the following main contributions: (1) the development of a technique to perform a quick and accurate estimation of the stray magnetic field and losses of the tank when there is asymmetry in transformer windings; (2) characterisation of the stray magnetic field on the tank walls for a better visualization of shielding placement; and (3) study of the potential reduction in stray losses on tank walls and core clamps, through the adoption of shell-type configurations.

## 2. Modelling and Considerations

### 2.1. Geometric Model of Column-Type Transformers

Additional losses in all structural components in the transformer sometimes represent more than 20% of the load losses if they are not controlled [21]. Most of the additional losses occur in the tank, so this work lays more emphasis on this part and its control through magnetic shunts. Additional losses in core clamps or yoke beams are also considered, but

the analysis of these losses in structural parts such as guides and flitch plates was discarded. Figure 1a shows the actual arrangement of the transformer tank being analysed, equipped with magnetic shunts. Figure 1b shows the geometric model used for the analysis, covering the structural components and their positioning. In particular, tank details are omitted to improve clarity of magnetic shunts and visualisation of core clamps. It is important to highlight that in this model the core is represented as a solid piece, without considering laminations. This simplification arises from the fact that the main focus of the research is the analysis and calculation of losses in the magnetic shunts and the tank. Figure 1c represents an overhead view of a cross section that includes the tank walls: front wall (Fw), left wall (Lw), rear or back wall (Bw), and right wall (Rw). The top (Tw) and the bottom (Gw) tank walls are also considered. The separation of tank walls allowed us to analyse in greater detail the amount of stray magnetic flux in each of the walls. Other parameters include primary winding height ( $h_p$ ) and thickness ( $w_p$ ), secondary winding height ( $h_s$ ) and thickness ( $w_s$ ), and magnetic shunt height ( $h_{sh}$ ).

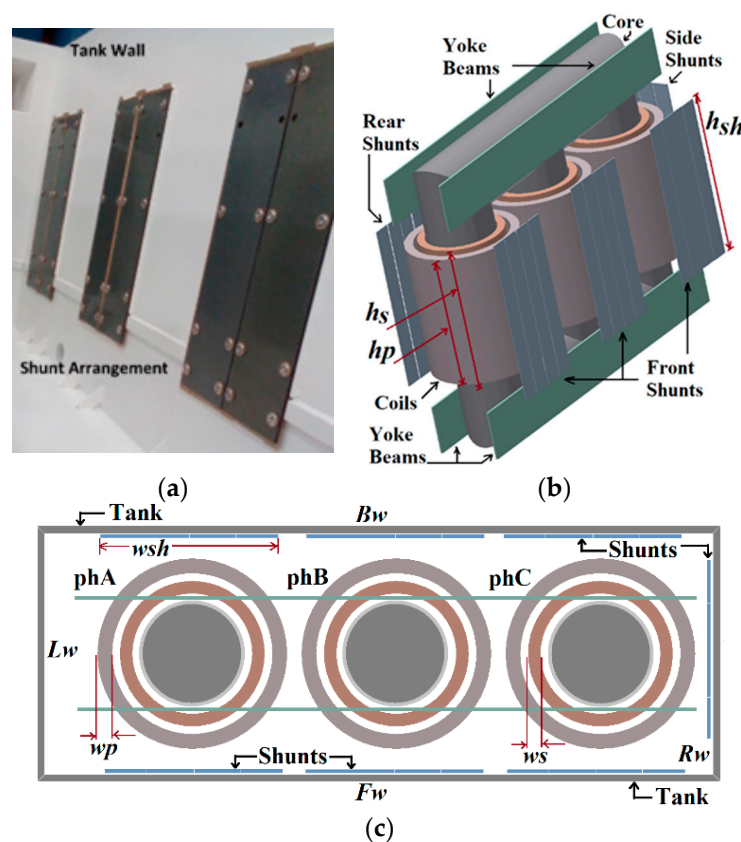


**Figure 1.** Geometry model of the three-phase transformer analysed for stray losses: (a) real arrangement, (b) 3D view of the components, and (c) top view with tank walls nomenclature.

### 2.2. Modelling Additional Losses

The measurement of stray losses in the transformer tank walls does not differentiate between hysteresis, eddy, and excess losses. We isolated each of the six walls, treating them as individual mild steel sheets. This simplification facilitates a more detailed analysis of stray losses. The value of  $|B_d|$  is derived through electromagnetic simulations using the Finite Element Method (FEM). Specifically, for calculating the loss components within the laminations of the ferromagnetic material, the methodology of this study aligns with the conceptual framework introduced in [22]. This strategic separation and focused analysis enhances the precision in evaluating the distinct contributions of hysteresis, eddy and

excess losses in the transformer tank walls. The hysteresis loss density (Watts/m<sup>3</sup>) in each of the tank walls will be given by the Steinmetz equation [23]:

$$P_h = k_h B_d^\alpha f, \tag{1}$$

where  $k_h$  is a hysteresis factor that depends on the properties of the material with which the tank wall is made,  $k_h = 63$  for mild steel commonly used for transformer tanks,  $\alpha$  is the Steinmetz coefficient (the value of Steinmetz coefficient  $\alpha$  is approximately 2 for all modern magnetic materials) and  $f$  is the operating frequency. The additional loss density (Watts/m<sup>3</sup>) due to eddy losses can be determined by [22] the following:

$$P_e = \frac{1}{6} \sigma \pi^2 B_d^2 f^2 q^2, \tag{2}$$

where  $\sigma$  is the conductivity of the tank wall (In this case,  $\sigma = 6.67 \times 10^6$  S/m for mild steel) and  $q$  is the wall thickness. The additional loss density (Watts/m<sup>3</sup>) due to excess losses can be determined by [22] the following:

$$P_x = 8.76 \sqrt{\sigma G V_0 S} B_d^{1.5} f^{1.5}, \tag{3}$$

where  $S$  is the cross section of the tank wall and  $G$  and  $V_0$  are dimensionless constants related to the quality of the ferromagnetic material with which the tank wall is made. For example, for M4 (0.27 mm), grain-oriented steel  $G = 0.1356$  and  $V_0 = 0.0110$  at 1.5 T and 60 Hz, the excess losses in the tank walls were not considered in this work; however, it is possible to calculate them with this proposed technique by finding the  $|B_d|$  that reaches the tank wall. Moreover, determining the values of  $G$  and  $V_0$  of the tank wall would be outside the scope and technical feasibility of this work.

Equations (1)–(3) represent the density of losses per unit volume, so they need to be multiplied by the volume  $V$  of each wall to obtain the losses. The additional plate losses of the magnetic shunts can be calculated in the same way using (1)–(3), taking into account that the values of the coefficients  $k_h$ ,  $\sigma$ ,  $G$  and  $V_0$  change depending on the material used. Mild steel is used for the tank and yoke beams, while grain-oriented silicon steel (GOES) and amorphous silicon steel were analysed to be used for the magnetic shunts.

### 2.3. Stray Losses Modelling with FEM

Analysing the stray magnetic flux  $\phi d$  and its density  $B_d$  along with the extra losses in the tank and structural components using the Finite Element Method (FEM) requires the computation of induced losses attributed to eddy current ( $P_e$ ), excluding hysteresis. To achieve this, a model founded on the solution of the magnetic vector potential  $\mathbf{A}$  in the frequency domain [24,25] was used. The expressions for this model are as follows:

$$j\omega\sigma\mathbf{A} + \nabla \times \left( \frac{1}{\mu} \nabla \times \mathbf{A} \right) - \mathbf{J}_e = 0, \tag{4}$$

$$P_e = \frac{1}{2} Re \left[ \sum_{i=1}^n (\rho_i J_{ei}^* J_{ei}) V_i \right], \tag{5}$$

where variable  $n$  represents the number of elements. Each component contributing to the tank, including the tank walls and magnetic shunts, is characterised by a volume denoted as  $V_i$ . Furthermore,  $\rho_i$  stands for the diagonal matrix incorporating the resistivity values specific to the materials constituting each element. Additionally,  $J_{ei}$  represents the induced current density vector resulting from the stray or stray magnetic field.

### 3. Assessment and Model of the Stray Magnetic Field

For determining the stray magnetic field and the associated losses within the tank walls and other ferromagnetic structural components of the transformer, it is necessary to

solve Equations (4) and (5) in a three-dimensional (3D) space within the frequency domain. To accomplish this, the Magnetic Fields module of COMSOL Multiphysics was used as the chosen simulation tool for this study. Complementary information of the simulation included the following: around 1,915,500 mesh elements were used (shunts included), the solution time was 88 min 27 s, the virtual memory used was 11.3 GB, Intel64 family computer equipment was used, and there was 16.32 GB RAM available, 6 cores, 3.2 GHz.

### 3.1. Assessment of the Stray Magnetic Field Density on Tank Walls

The magnitudes of  $|B_d|$  on the tank wall can be examined in Figure 2a, excluding the influence of magnetic derivations. For clarity, wall dimensions ( $L_w$  and  $T_w$ ) have been omitted for better visualisation. In particular, the maximum values of  $|B_d|$ , which reach 0.9 T, are concentrated in the centre of the  $R_w$  side wall. This concentration is attributed to its proximity to the coil. Walls  $F_w$  and  $B_w$  are shown with a low value of  $|B_d| = 0.4$  T at the centre of the wall. Figure 2b shows the characterised curve of  $|B_d|$  on the tank walls. Figure 3a shows the values of  $|B_d|$ , considering vertically placed magnetic leads. In this configuration,  $|B_d|$  on the tank walls can be reduced to 0.2 T, while the walls of the magnetic shunts have higher values of 0.9 T.

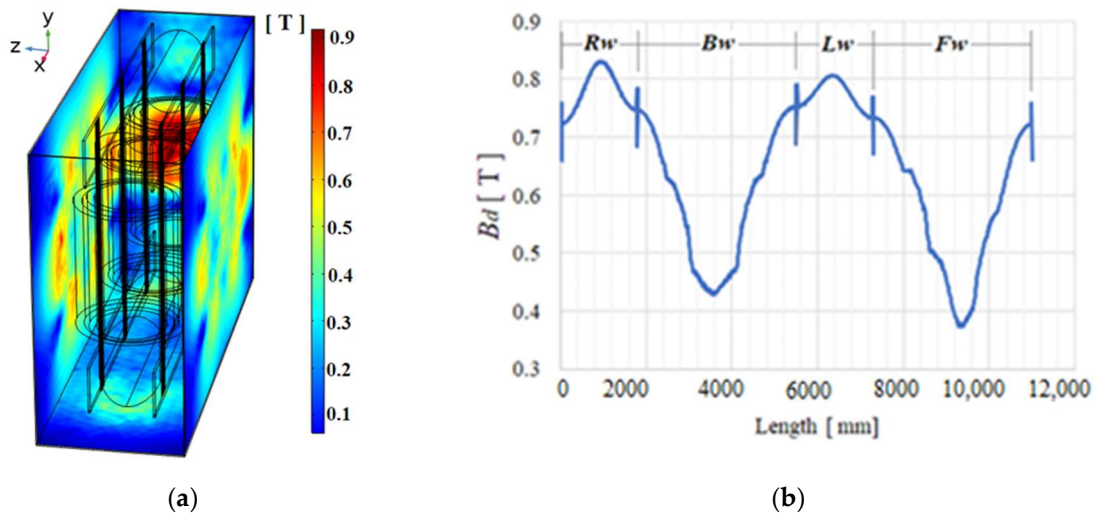


Figure 2. Without magnetic shunts: (a) stray magnetic flux density  $|B_d|$  norm at tank walls; (b) characterisation of  $|B_d|$ .

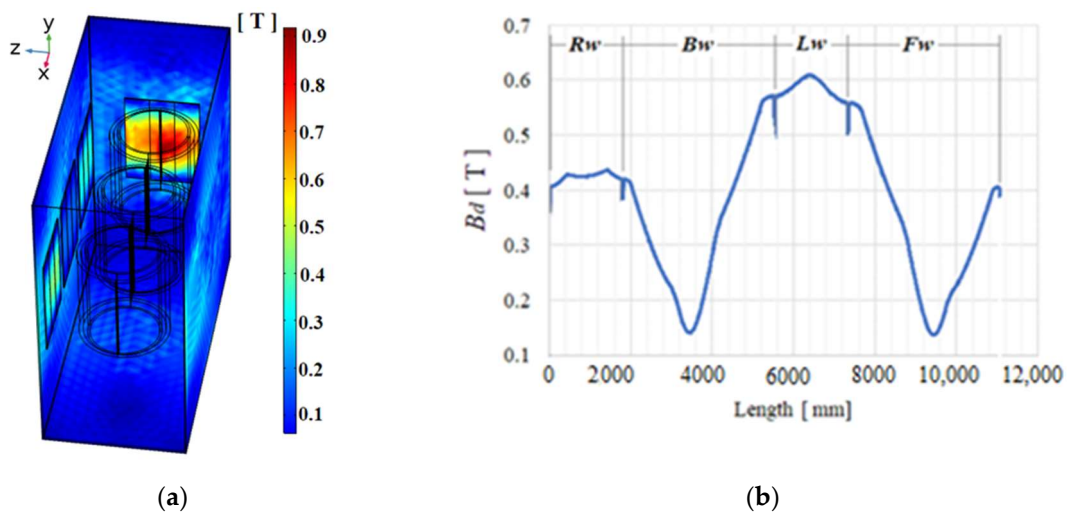
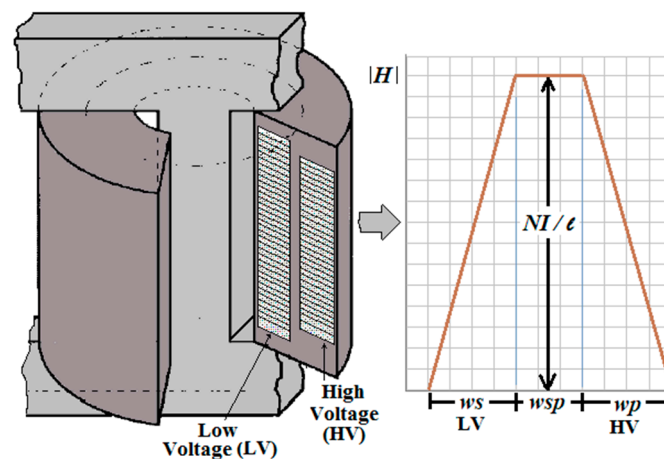


Figure 3. With magnetic shunts: (a) stray magnetic flux density  $|B_d|$  norm at tank walls; (b) characterisation of  $|B_d|$ .

The characterisation of  $|B_d|$  on the tank walls protected by magnetic shunts is shown in Figure 3b; magnetic shunts thickness and gap separation with the tank were the same 9 mm (3/8"). In particular, wall  $L_w$  keeps  $|B_d|$  at elevated values, since it remains unprotected by derivations. On the contrary, the values of  $|B_d|$  on the wall  $R_w$  decreases to 0.4 T. This reduction depends on the type of material and the thickness of the shunts. In this case, magnetic shunts of the same core material, specifically GOES Steel, were used and simulated. The root mean square (rms) value of  $|B_d|$  in the absence of shunts was 0.68 T. After adding shunts, the rms values of  $|B_d|$  decreased to levels as low as 0.4 T, representing a substantial 41.1% reduction in  $|B_d|$  on the walls of the tank.

### 3.2. Impact of Winding Asymmetry

The dimensions of the transformer windings, including height and width, play an important role in setting the magnitudes of  $|B_d|$  that reach the tank wall and other ferromagnetic structural elements. These dimensions, in turn, influence additional losses. Consequently, this study evaluates the effects of winding geometric asymmetry on the values of  $|B_d|$ , examining the balance of the magnetic field intensity  $|H|$  that arises from the geometry of the windings. For the designers, it is evident that they will seek to centre the windings; however, it is not evident what effect would be caused to the "magnetic centre" by this geometric asymmetry of the windings, so this impact must be analysed and shown so that the designer can take precautions when they estimate the stray magnetic flux that reaches the tank walls and core clamps. In an ideal two-winding transformer, the magnetic field intensity  $|H|$  exhibits an isosceles trapezoidal characteristic, as shown in Figure 4. This ideal condition is achieved when the heights and thicknesses of both windings are equal ( $h_s = h_p$  and  $w_s = w_p$ ), which is often observed in transformers with a 1:1 ratio. During the transformer design process, efforts are made to balance the ampere-turns of both windings. However, due to geometric complexities, variations in conductor dimensions and manufacturing adjustments, winding heights and thicknesses may differ. This deviation results in a scalene trapezoidal feature in  $|H|$ .



**Figure 4.** Ideal isosceles trapezoidal characterisation of  $|H|$  between the coils of a typical two-winding transformer. It can be seen that the field intensity is uniform and greater in the space between the windings. It shows a homogeneous and completely trapezoidal distribution (own authorship).

The variation in  $|H|$  serves as a key parameter to determine the strength of the scattered magnetic field with  $|H_d|$  reaching the core walls and other components. To explore this effect, several cases were analysed to determine the corresponding values of  $|H_d|$  and  $|B_d|$  that impact the walls of the tank. The results of these analyses are presented in Figure 5, which provides a complete visual representation of the various scenarios considered in this study. Case 1 is the ideal design ( $h_p = h_s$ ,  $w_p = w_s$ ). The parameters of other cases are mentioned as follows: Case 2, ( $h_p = 0.85 \cdot h_s$ ,  $w_p = w_s$ ), Case 3 ( $h_p = 0.85 \cdot h_s$ ,  $w_p = 1.15 \cdot w_s$ ) and Case 4 ( $h_p = 0.85 \cdot h_s$ ,  $w_p = 1.30 \cdot w_s$ ).

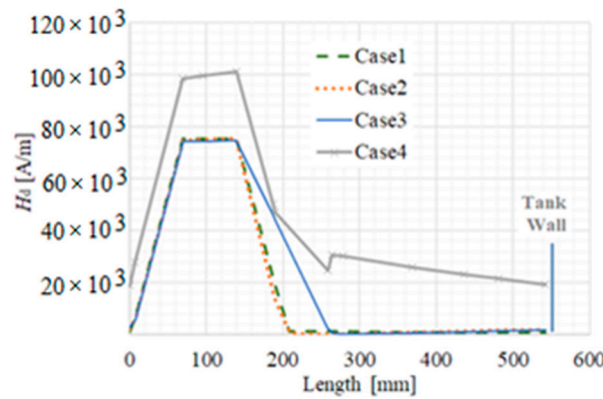


Figure 5. Trapezoidal characterisation of  $|H|$  for different cases analysed.

These cases were considered in a very general way to visualise the impact of the geometric asymmetry of the windings. Analysing and addressing a very specific case could be the content of another work; an example of a specific case could be when tap changers are added. Taps with a wide voltage regulation range, sometimes outside the standards (NFPA-70, IEC-60364-1)  $\pm 5\%$ , implies including more turns and having ampere-turns causes unbalances in the coil, which produces a magnetic unbalance between the coils and increases the stray magnetic field. Case 4 is a common scenario encountered in practical transformer design, where efforts are made to achieve a balance in winding dimensions. Despite these attempts, there is a disparity in both the heights and thicknesses of the windings. Regardless of the specific case, this variation in dimensions directly influences the magnitudes of  $|H_d|$ ,  $|B_d|$ , consequently contributing to additional losses experienced in the tank walls.

### 3.3. Model to Determine Stray Magnetic Field on Tank Walls

In order to calculate the additional losses that occur in the tank walls, Equations (1)–(3) are used. However, it is necessary to first determine the effective value of  $|B_d|$ . Through the analysis performed to characterise  $|H|$  and the large amount of information obtained through finite element method (FEM) simulations and with the intention of helping the designer to estimate the stray magnetic field due to the magnetic imbalance as well as the geometric asymmetry of the windings, a model has been successfully derived. This model facilitates the estimation of the magnitude of  $|H|$  (expressed in A/m) and is expressed as follows:

$$H_e = \frac{1}{K_R} \left| \left( \frac{N_s I_s}{h_s} - \frac{N_p I_p}{h_p} \right) \right|, \tag{6}$$

where  $N_p$ ,  $N_s$ ,  $I_p$  and  $I_s$  are turns and currents of the primary and secondary windings, respectively,  $h_p$ ,  $w_p$ ,  $h_s$  and  $w_s$  are heights and widths of the primary and secondary windings, respectively and  $K_R$  is calculated by the Rogowski factor given by [26] the following:

$$K_R = 1 - \left( \frac{w_p + w_{sp} + w_p}{\pi h w} \right) \left( 1 - e^{\frac{-\pi h w}{(w_p + w_{sp} + w_p)}} \right), \tag{7}$$

where  $hw$  is the height of the core window. It is proposed that the estimation of the magnitude of  $|H_d|$  at a distance  $d$  from the external winding (high voltage winding) of the coil is given by the following:

$$H_d = H_e \left( e^{\frac{-d}{(w_p + w_{sp} + w_p)}} \right), \tag{8}$$

Afterwards, the density of the magnetic field that reaches the walls of the tank would be given by the following:

$$B_d = \left( e^{\frac{-d}{(w_p + w_{sp} + w_p)}} \right) H_e \mu_r \mu_0, \tag{9}$$

where  $\mu_r$  is the relative permeability and  $\mu_0 = 4\pi \times 10^{-7}$ . From (6)–(9), it is possible to show that the proposed technique seeks to determine the stray magnetic field based on the difference in the magnetomotive force (ampere-turns) produced by each winding and thereby later determine the magnetic field density that will reach the tank walls at a distance  $d$  from the coil.

#### 4. Design Parameters and Loss Values

##### 4.1. Estimation of Stray Losses with FEM and with the Proposed Model

To compare the results obtained from the Finite Element Method (FEM) simulations with those derived from the proposed model, load tests were carried out on a 25 MVA power transformer operating at 115 kV–34.5 kV, with Delta-connection. The complementary values of the design and manufacturing parameters of the transformer are presented in Table 1. It should be noted that the losses per phase in the low voltage winding amounted to approximately 43.75 kW, while those in the high voltage winding were around 57 kW. Core losses were measured at approximately 21.7 kW, resulting in an overall transformer efficiency of approximately 98.5% at full load. From these measured loss values and considering efficiency, it was determined that the estimated additional losses would be approximately 35.6 kW. It is worth noting that this value of additional losses cannot be measured directly, much less separated between those attributed to the tank and those associated with the support structures. However, these losses can be estimated based on the total losses measured. Table 2 provides the losses obtained by electromagnetic simulations using finite element analysis for the tank walls and yoke beams.

**Table 1.** Design and manufacturing parameters of 25 MVA transformer.

| Design Parameter                 | Value  |
|----------------------------------|--------|
| Core window high (mm)            | 1482   |
| LV—Margins (mm)                  | 89     |
| HV—Margins (mm)                  | 89     |
| Core Diameter (mm)               | 552    |
| LV—HV Space (mm)                 | 51     |
| Tank Wall Thickness (mm)         | 9.5    |
| Core-LV winding distance (mm)    | 19     |
| Rw wall-HV winding distance (mm) | 381    |
| Fw wall-HV winding distance (mm) | 330    |
| LV width (mm)                    | 69.8   |
| LV height (mm)                   | 1219.2 |
| HV width (mm)                    | 123.8  |
| HV height (mm)                   | 960    |
| Volts/Turns                      | 23.00  |

**Table 2.** Stray or additional losses and  $|B_d|$  estimation.

| Losses             | By FEM | $ B_d $ by FEM | By (9 & 2) |
|--------------------|--------|----------------|------------|
| Lw, left side wall | 6455 W | 0.520 T        | 6853 W     |
| Rw right side wall | 6853 W | 0.528 T        | 7262 W     |
| Fw, front wall     | 8322 W | 0.534 T        | 7694 W     |
| Bw, rear wall      | 7694 W | 0.520 T        | 7091 W     |
| Bottom wall        | 2517 W | 0.493 T        | 2271 W     |
| Top wall           | 906 W  | 0.420 T        | 1063 W     |
| Top yoke beams     | 1252 W | 0.600 T        | 1252 W     |
| Bottom yoke beams  | 1634 W | 0.680 T        | 1634 W     |

The additional losses in the tank walls amounted to 32.23 kW and the losses in the yoke beams were calculated to be 1.84 kW, resulting in an estimated total additional loss of 34.0 kW using Equation (2). In contrast, finite element method (FEM) simulations yielded a total additional loss of 34.40 kW. The discrepancy between these values and those obtained by measurement is approximately 3.3% to 3.5%.

The third column of Table 2 shows the effective values of the magnetic field density estimated by FEM, as illustrated by the characteristic curve on the walls in Figure 2b. In particular, employing both FEM and the proposed model (Equation (9)) allows detailed quantification of losses in each tank wall and facilitates the determination of losses in the metallic elements that support the core, such as the yoke beams. The introduction of magnetic shunts is seen in the reduction of losses. The obtained values have been summarised in Table 3. According to FEM estimates, the total additional losses with magnetic shunts are 19.70 kW, while the proposed model (Equation (9)) indicates the losses of 19.0 kW, which means a notable loss reduction of approximately 42%.

**Table 3.** Stray losses and  $|B_d|$  estimation with magnetics shunts.

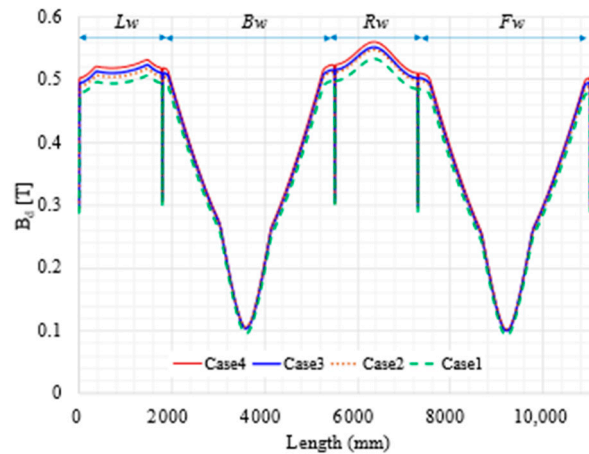
| Losses             | By FEM | $ B_d $ by FEM | By (9 & 2) |
|--------------------|--------|----------------|------------|
| Lw, left side wall | 6853 W | 0.520 T        | 6455 W     |
| Rw right side wall | 3457 W | 0.428 T        | 2720 W     |
| Fw, front wall     | 3151 W | 0.322 T        | 3199 W     |
| Bw, rear wall      | 2814 W | 0.320 T        | 3151 W     |
| Bottom wall        | 1565 W | 0.324 T        | 1651 W     |
| Top wall           | 624 W  | 0.211 T        | 697 W      |
| Top yoke beams     | 530 W  | 0.266 T        | 499 W      |
| Bottom yoke beams  | 704 W  | 0.299 T        | 632 W      |

#### 4.2. Estimation of the Impact of Winding Asymmetry

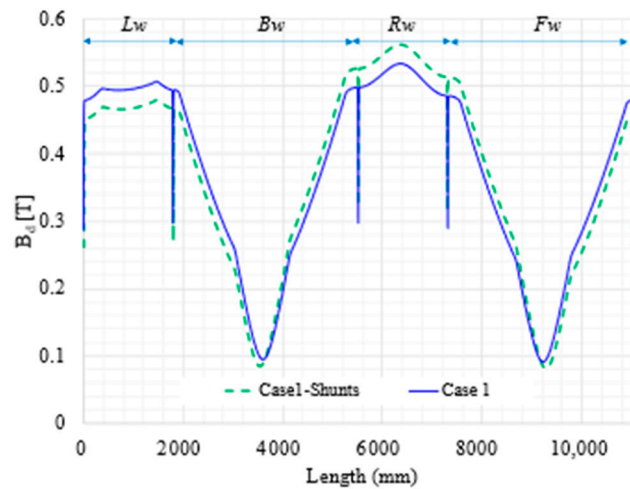
The study used Finite Element Method (FEM) simulation and the proposed simple model (2) to assess the impact of asymmetry in transformer windings as well as to estimate losses associated with different heights and widths. Figure 6 illustrates magnetic field values obtained through FEM without magnetic shunts around the tank walls, showcasing variations in winding heights and widths. Case 4 characterised by larger dimensions of the outer winding (high-voltage winding) compared to the low-voltage winding yielded the highest values for stray magnetic fields. Conversely, Case 1, representing the ideal scenario with identical heights and widths for all windings, demonstrated the lowest values for stray magnetic fields. In Figure 7, a comparison for Case 1 reveals field values with and without magnetic shunts. Notably, the presence of magnetic shunt protection along certain walls led to a decrease in stray magnetic fields. However, in areas without protection, such as the left wall (Lw), the stray magnetic field increased. This observation underscores the effectiveness of magnetic shunts in reducing losses and highlights their practical utility in transformer design.

Table 4 presents a compilation of results derived from varying the heights and thicknesses of the windings for the purpose of visualising their impact. Parameters Tyb and Byb were added, denoting Top yoke beams and Bottom yoke beams, respectively. The findings indicate that when the design aims for equal dimensions in both height and width, there is a noticeable reduction in the stray magnetic field. Consequently, this reduction contributes to a decrease in additional losses, amounting to approximately 4.2%. On the contrary, during the design phase, when the high voltage winding is configured with greater height and width than the low voltage winding, it results in an increase in the stray magnetic field. As a consequence, additional losses also increase, reaching approximately 16.1% in comparison to the ideal case (Case 1) and around 11.2% in the real case. The results, detailed in Table 5, demonstrate a consistent trend of magnetic shunts effectively contributing to a reduction in losses, achieving a significant decrease of around 44.2%. Figure 8 depicts the values of  $|B_d|$  obtained through the proposed model (6)–(9) for both the real case and case 2. Notably, the values of  $H_e$  and  $|H_d|$  were determined as

$7.69 \times 10^4$  A/m and  $1.63 \times 10^4$  A/m, respectively. This implies that this magnetic field strength would be present at a distance  $d$ —specifically at the edge of the right wall  $R_w$  of the tank ( $d = 381$  mm). It is essential to clarify that the proposed model does not account for the ideal case due to the low probability of achieving symmetry in winding dimensions during manufacturing.



**Figure 6.** Without magnetic shunts' varying height and width of windings. Case 1 ( $h_p = h_s$ ,  $w_p = w_s$ ); Case 2 ( $h_p = 0.85 \cdot h_s$ ,  $w_p = w_s$ ); Case 3 ( $h_p = 0.85 \cdot h_s$ ,  $w_p = 1.15 \cdot w_s$ ); and Case 4 ( $h_p = 0.85 \cdot h_s$ ,  $w_p = 1.15 \cdot w_s$ ).



**Figure 7.** With magnetic shunts' varying height and width of windings. Case 1 ( $h_p = h_s$ ,  $w_p = w_s$ ); Case 2 ( $h_p = 0.85 \cdot h_s$ ,  $w_p = w_s$ ); Case 3 ( $h_p = 0.85 \cdot h_s$ ,  $w_p = 1.15 \cdot w_s$ ); and Case 4 ( $h_p = 0.85 \cdot h_s$ ,  $w_p = 1.15 \cdot w_s$ ).

**Table 4.** Stray losses (W) without magnetics shunts.

|        | Lw   | Rw   | Fw   | Bw   | Gw   | Tw   | Tyb  | Byb  |
|--------|------|------|------|------|------|------|------|------|
| Case 1 | 6171 | 6579 | 7972 | 7348 | 2416 | 868  | 1202 | 1569 |
| Case 2 | 6352 | 6757 | 8181 | 7532 | 2472 | 891  | 1226 | 1603 |
| Real   | 6455 | 6853 | 8322 | 7694 | 2517 | 906  | 1252 | 1634 |
| Case 3 | 6958 | 7388 | 8996 | 8325 | 2711 | 978  | 1350 | 1763 |
| Case 4 | 7165 | 7600 | 9287 | 8540 | 2814 | 1013 | 1396 | 1812 |

**Table 5.** Stray losses (W) with magnetics shunts.

|        | Lw   | Rw   | Fw   | Bw   | Gw   | Tw  | Tyb | Byb |
|--------|------|------|------|------|------|-----|-----|-----|
| Case 1 | 6565 | 3388 | 3025 | 2699 | 1534 | 603 | 524 | 682 |
| Case 2 | 6750 | 3419 | 3107 | 2761 | 1552 | 617 | 529 | 692 |
| Real   | 6853 | 3457 | 3151 | 2814 | 1565 | 624 | 537 | 704 |
| Case 3 | 7394 | 3734 | 3416 | 3050 | 1690 | 680 | 581 | 760 |
| Case 4 | 7627 | 3837 | 3523 | 3129 | 1751 | 699 | 599 | 781 |

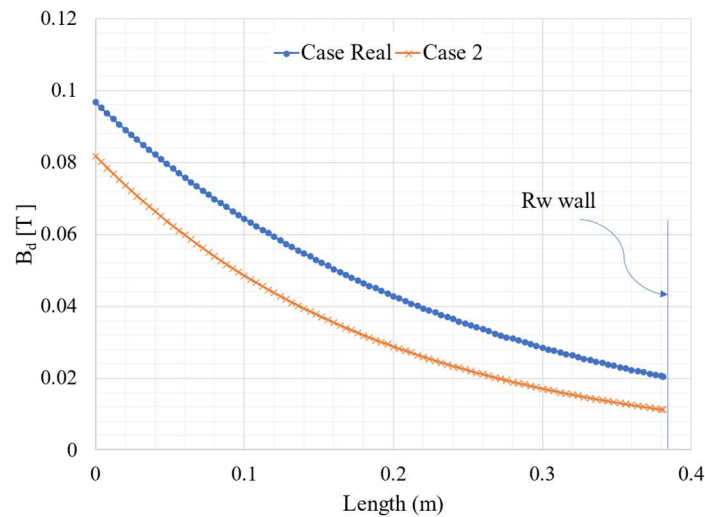


**Figure 8.** Magnetic Flux Density Distribution from HV winding to Rw wall.

#### 4.3. Materials for Magnetic Shunts

Three materials, namely Mill anneal electrical steel, Electrical Silicon Steel Grain Oriented (CRGO) and Amorphous Steel, were reviewed and analysed using finite element method (FEM) simulation. Mill Steel served as a reference point, with an approximate cost of \$1200 per ton. It possesses a relative permeability of 2000 and a resistivity of  $0.143 \mu\Omega\text{m}$ , for CRGO  $0.48 \mu\Omega\text{m}$  and Amorphous Steel  $1.3 \mu\Omega\text{m}$ , remembering that the relative permeability of these latter materials depends on their B–H curve. It is important to clarify that the manufacturer of these magnetic shunts uses scrap or residual material from the manufacturer of the core; the material was not purchased for this purpose. Also, the amorphous material is very fragile and difficult to work with, so it is rarely used as a shield for the tank, but it was considered to be analysed in this work since it is also in the scrap material from the cores.

To standardise the sizing of the magnetic shunt plates and facilitate an objective comparison among the considered materials, the widely recognised magnetic field penetration formula [27] was employed. This approach ensures a systematic evaluation based on the thickness of the shunt plates, allowing for a comprehensive assessment of their performance characteristics.

$$\delta = \sqrt{\frac{\rho}{\mu\pi f}}, \tag{10}$$

where  $\rho$  is the material resistivity,  $\mu$  is the permeability of the material and  $f$  is the operating frequency of the transformer. Taking into account a magnetic shunt plate with a thickness of 1 mm, Figure 9a illustrates the magnetic field distribution across a 1 mm thick steel sheet for the various materials under analysis, accompanied by visible magnetic field lines. To enhance the clarity of the magnetic field distribution values within the magnetic shunts, a more detailed presentation has been provided in Figure 9b. Observing Figure 9b, it is evident that CRGO Electrical Steel exhibits a higher magnetic field absorption compared to other materials. However, its cost is higher than that of Mill anneal steel, which has garnered more popularity as a magnetic shunt material owing to its cost-effectiveness

and satisfactory absorption capacity. On the other hand, the amorphous material sheet is recognised for its excellence in transformer core development due to its high permeability and resistivity, resulting in minimised electrical losses. Nevertheless, creating magnetic shunts using amorphous material is not technically or economically feasible due to its limited magnetic field penetration capacity as the format is incorrect.

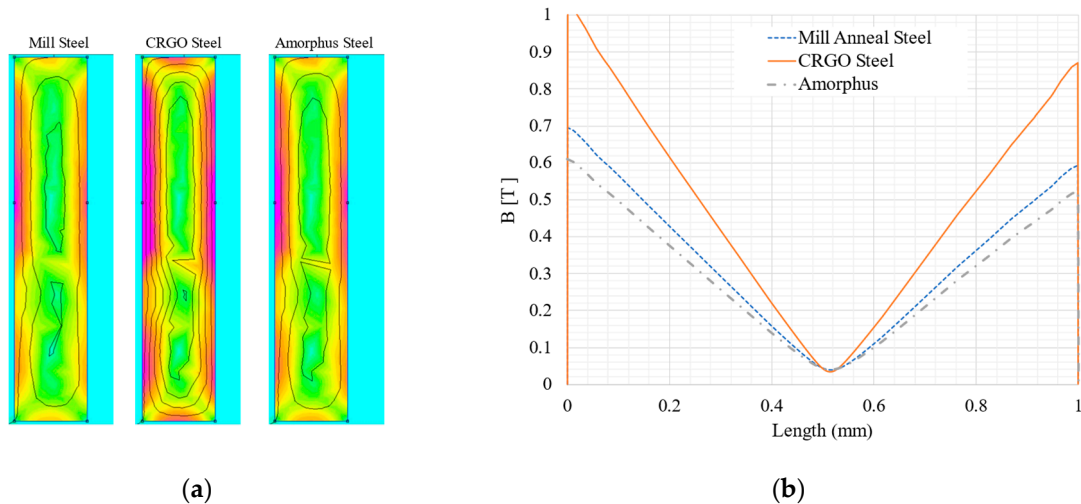


**Figure 9.** Comparison of stray magnetic field absorption: (a) stray magnetic flux density at magnetic shunt 1 mm; (b) characterization of  $|B|$ .

### 5. Impact of Shell-Type Configuration on Additional Losses

Transformer manufacturers widely recognise the shell-type configuration as an effective method to mitigate the stray of the magnetic field and, consequently, reduce additional losses. Despite its significance, the quantification of these benefits has not received widespread promotion. In Figure 10, the model of the shell-type configuration and its analysis path for a pad-mounted-type distribution transformer are depicted. The design and manufacturer parameters for the analysed 1500 kVA shell-pad-mounted transformer are detailed in Table 6. Noteworthy characteristics include a Delta connection at 22.5 kV in the primary winding, a 220/127 V square core cross section, an average magnetic field of 1.6 T in the core and an efficiency of 99% for the shell type compared to 98.8% for the core type. Figure 11 shows the magnetic field distribution in the active elements (core and coils) as well as on the tank walls of the shell-type transformer. In this representation, the average magnetic field in the core is approximately 1.6 T, while on the tank walls, the average field is around 300 mT, with darker spots reaching 350 mT in areas where the active elements are close to the walls.

Figure 12 shows a comparison of the magnetic field distribution along an analysis path for a 1500 kVA core-type pad mounted I transformer (represented by the solid blue line) and a shell-type transformer (represented by the dotted green line). Notably, the core-type transformer exhibits a shorter analysis path due to its shorter front and rear walls in comparison to the shell type. Furthermore, the magnetic field values for the core type are higher on the tank walls, reaching approximately 410 mT. In contrast, the shell type registers its highest magnetic field value around 350 mT, signifying a 14% reduction in the stray magnetic field reaching the magnetic tank. While this reduction would ideally correspond to a proportional decrease in additional losses, it is essential to consider that the tank for the shell-type transformer is longer to accommodate the active elements. As a result, the anticipated reduction in losses is more modest, estimated to be in the range of 6% to 8%. Table 7 provides results obtained through the finite element method (FEM) and the proposed model (9), facilitating a comparison and confirming the effectiveness of reducing stray losses in the transformer tank with the adoption of a shell-type configuration. It must be clarified that although it is observed that stray losses are lower in the shell-type

configuration, there are other elements that must be taken into account while designing and estimating total losses in the transformer. In a shell-type configuration, the core grows, and the no-load losses will be greater. In terms of manufacturing, its cost increases along with the increase in manufacturing time and materials volume; however, this work focuses on highlighting the decrease in the stray magnetic field. Consequently, a decrease in stray losses in the tank walls and core clamps is needed for the designer to have an idea of the impact of the stray loss reduction with the shell configuration and to make a decision for its manufacturing.

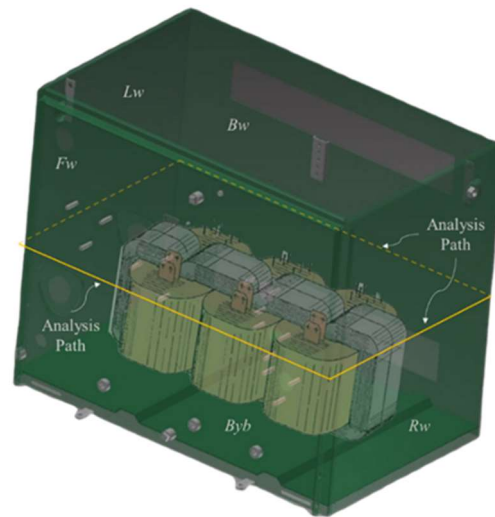


Figure 10. Shell-type transformer with analysis path to estimate the stray flux and its impact.

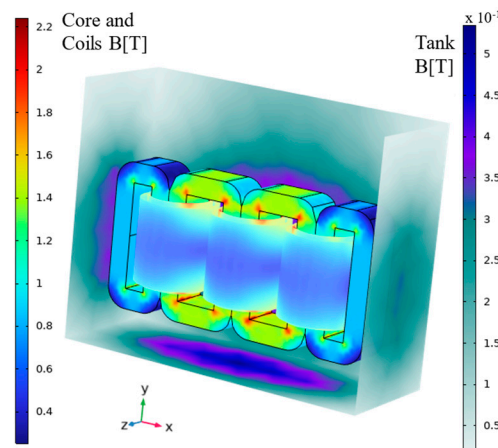


Figure 11. Tank, core and coils B distribution simulation of shell-type transformer.

Table 6. Core- and shell-type pad-mounted transformer design and manufacturing parameters.

| Design Parameter                 | Shell Type | Core Type |
|----------------------------------|------------|-----------|
| Core Window High (mm)            | 274        | 274       |
| LV—Margins (mm)                  | 20         | 20        |
| HV—Margins (mm)                  | 40         | 40        |
| Core Length (mm)                 | 237        | 237       |
| LV—HV Space (mm)                 | 10         | 10        |
| Tank Wall Thickness (mm)         | 4.7        | 4.7       |
| Core-LV Winding Distance (mm)    | 4          | 4         |
| Rw wall-HV Winding Distance (mm) | —          | 38.1      |
| Rw wall-Core leg Distance (mm)   | 25.4       | —         |
| Fw wall-HV Winding Distance (mm) | 40         | 40        |
| LV Width (mm)                    | 55         | 55        |

Table 6. Cont.

| Design Parameter | Shell Type | Core Type |
|------------------|------------|-----------|
| LV High (mm)     | 274        | 274       |
| HV Width (mm)    | 42         | 42        |
| HV High (mm)     | 234        | 234       |
| Volts/Turns      | 22.8       | 22.8      |
| Tank Length (mm) | 2121       | 1964      |
| Tank Width (mm)  | 1370       | 1370      |
| Tank Height (mm) | 1760       | 1960      |

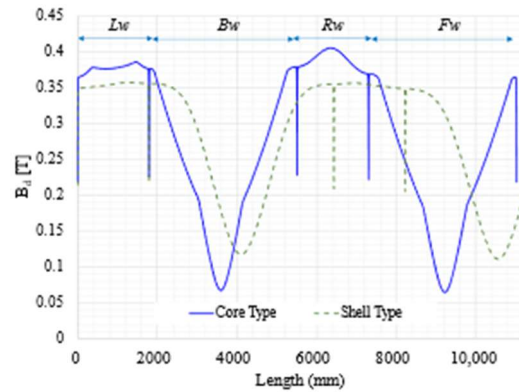


Figure 12. Magnetic flux density core-type and shell-type comparison.

Table 7. Stray losses for shell and core type.

|                    | Shell Type |            | Core Type |            |
|--------------------|------------|------------|-----------|------------|
|                    | By FEM     | Bd  by (2) | By FEM    | Bd  by (2) |
| Lw, left side wall | 218.0 W    | 231.4 W    | 295.9 W   | 314.8 W    |
| Rw right side wall | 217.9 W    | 230.9 W    | 289.2 W   | 312.9 W    |
| Fw, front wall     | 422.2 W    | 390.3 W    | 412.9 W   | 451.3 W    |
| Bw, rear wall      | 388.6 W    | 358.1 W    | 405.4 W   | 442.6 W    |
| Bottom wall        | 308.9 W    | 278.7 W    | 286.4 W   | 315.4 W    |
| Top wall           | 181.7 W    | 213.2 W    | 220.8 W   | 242.6 W    |

## 6. Conclusions

Reducing additional losses in transformers implies having a competitive advantage in the business of designing and manufacturing transformers. Some important technical literature is available on this topic; however, even in the design stage there are disadvantages such as computational resources and time for performing simulations with FEM to determine the stray magnetic field. This study has addressed this challenge, highlighting the impact that designing and manufacturing asymmetric coils has on the stray magnetic field. It has also addressed the challenge of showing an easy-to-use and low computational cost technique in the design stage to determine the magnetic field that would reach the tank walls and consequently the stray losses that are induced. The proposed technique was compared with the simulations carried out in a commercial FEM programme. From Section 4.1, with the measured values, the difference in the results was 3%, so this value can help with trusting its utilisation.

Also in this work, in addition to estimating the magnetic field on the tank walls, the magnetic field that reaches these walls was characterised, allowing for the visualisation and understanding of its behaviour with the purpose of estimating the thickness of the magnetic shunt plates and the best position to place them. It was demonstrated that the placement of the magnetic shunts allows the tank stray losses to be reduced by up to 40%. It was also evident that if the thickness and heights of the windings, in the design stage, are sought to be more equal, stray magnetic fields can be avoided, and consequently, stray

losses on the tank walls can be reduced by 11%. It is possible to further reduce losses by using other accessories for the tank such as non-magnetic stainless steel; however, this work focused on determining the impact of using magnetic shunts to reduce stray losses. This work also demonstrates the advantage of using a shell-type configuration to reduce the magnetic field that hits the tank walls, demonstrating that this configuration by itself can reduce the stray losses of the tank walls up to 14%. However, it should also be considered that the shell configuration can increase the size of the tank, which means that losses may only be reduced between 6% and 8%. In general, with the results and evidence shown in this work, useful information regarding the design and manufacturing of transformers has been presented.

**Author Contributions:** Conceptualization, I.A.H.-R. and X.G.-R.; methodology, I.A.H.-R. and J.C.O.-G.; validation, I.A.H.-R., J.C.O.-G. and R.O.-V.; formal analysis, I.A.H.-R., X.G.-R. and J.C.O.-G.; investigation, I.A.H.-R. and X.G.-R.; resources, X.G.-R. and R.E.-P.; data curation, R.O.-V.; writing—original draft preparation, I.A.H.-R. and X.G.-R.; writing—review and editing, X.G.-R., J.C.O.-G. and R.O.-V.; visualization, I.A.H.-R. and X.G.-R.; supervision, R.E.-P.; project administration, X.G.-R. and R.E.-P. All authors have read and agreed to the published version of the manuscript.

**Funding:** This research received no external funding.

**Data Availability Statement:** The original contributions presented in the study are included in the article, further inquiries can be directed to the corresponding author.

**Acknowledgments:** The authors are grateful for the financial support provided by the Consejo Nacional de Humanidades, Ciencia y Tecnología (CONAHCYT).

**Conflicts of Interest:** The authors declare no conflicts of interest.

## References

1. Liu, B.; Takahashi, Y.; Fujiwara, K.; Imamori, S. Stray Loss Evaluation of Power Transformers Using Simplified Air-Core Model With Tank and Frame. *IEEE Trans. Magn.* **2023**, *59*, 1–6.
2. Thango, B.A.; Jordaan, J.A.; Nnachi, A.F. Analysis of Stray Losses in Transformers using Finite Element Method Modelling. In Proceedings of the IEEE PES/IAS PowerAfrica, Nairobi, Kenya, 23–27 August 2021; pp. 1–5.
3. Nikkhoo, M.; Nasab, M.R.; Hosseini, A. An Innovative Shielding Strategy for Stray Loss Reduction of Neutral Grounding Reactor. *IEEE Trans. Magn.* **2022**, *58*, 1–9. [[CrossRef](#)]
4. de Oliveira, L.F.; Sadowski, N.; Cabral, S.H.L. Alternative model for computing transformer tank induced losses in the time domain. *IET Electr. Power Appl.* **2020**, *14*, 2507–2514. [[CrossRef](#)]
5. Drandić, A.; Frlić, S.; Trkulja, B. Methodology for Eddy Current Losses Calculation in Linear Variable Differential Transformers (LVDTs). *Sensors* **2023**, *23*, 1760. [[CrossRef](#)]
6. Orosz, T.; Pánek, D.; Karban, P. FEM Based Preliminary Design Optimization in Case of Large Power Transformers. *Appl. Sci.* **2020**, *10*, 1361. [[CrossRef](#)]
7. Olivares, J.C.; Cañedo, J.; Moreno, P.; Driesen, J.; Escarela, R.; Palanivasagam, S. Experimental Study to Reduce the Distribution-Transformers Stray Losses Using Electromagnetic Shields. *Electr. Power Syst. Res.* **2002**, *63*, 1–7. [[CrossRef](#)]
8. Vogel, F.J.; Adolphson, E.J. A stray loss problem in transformer tanks. *AIEE Trans. Power Appar. Syst.* **1954**, *73*, 760–764. [[CrossRef](#)]
9. Djurovic, M.; Monson, J.E. 3-Dimensional computation of the effect of the horizontal magnetic shunt on transformer leakage fields. *IEEE Trans. Magn.* **1977**, *13*, 1137–1139. [[CrossRef](#)]
10. Valkovic, Z. Calculation of the losses in three-phase transformer tanks. *IEEE Proc.* **1980**, *127*, 20–25. [[CrossRef](#)]
11. Djurovic, M.; Monson, J.E. Stray losses in the step of a transformer yoke with a horizontal magnetic shunt. *IEEE Trans. Power Appar. Syst.* **1982**, *101*, 2995–3000. [[CrossRef](#)]
12. Turowski, J.; Turowski, M.; Kopec, M. Method of three-dimensional network solution of leakage field of three-phase transformers. *IEEE Trans. Magn.* **1990**, *26*, 2911–2919. [[CrossRef](#)]
13. Koppikar, D.A.; Kulkarni, S.V.; Turowski, J. Fast 3-dimensional iterative computation of stray field and losses in asymmetric transformers. *IEEE Proc.* **2000**, *147*, 197–201.
14. Zhang, B.; Liu, L.; Liu, Y.; McVey, M.; Gardner, R.M. Effect of geomagnetically induced current on the loss of transformer tank. *IET Electr. Power Appl.* **2010**, *4*, 373–379. [[CrossRef](#)]
15. Diaz-Chacon, J.M.; Hernandez, C.; Arjona, M.A. Finite element and neural network approach for positioning a magnetic shunt on the tank wall of a transformer. *IET Electr. Power Appl.* **2016**, *10*, 827–833. [[CrossRef](#)]
16. Strac, L. Three-Phase Shunts for Stray Magnetic Field. *Procedia Eng.* **2017**, *22*, 183–188. [[CrossRef](#)]

17. Tsili, M.A.; Kladas, A.G.; Georgilakis, P.S.; Souflaris, A.T.; Pappas, D.G. Geometry optimization of magnetics shunts in power transformers based on particular hybrid finite-element boundary-element model and sensitivity analysis. *IEEE Trans. Magn.* **2005**, *41*, 1776–1779. [[CrossRef](#)]
18. Moghaddami, M.; Sarwat, A.I.; De Leon, F. Reduction of stray loss in power transformers using horizontal magnetic wall shunts. *IEEE Trans. Magn.* **2017**, *53*, 1–7. [[CrossRef](#)]
19. Magdaleno-Adame, S.; Penabad-Duran, P.; Olivares-Galvan, J.C.; Maximov, S.; Escarela-Perez, R.; Campero-Littlewood, E. Reduction of stray losses in Tertiary Voltage Bushings in power transformer tanks. In Proceedings of the 2014 IEEE International Autumn Meeting on Power, Electronics and Computing (ROPEC), Ixtapa, Mexico, 5–7 November 2014; pp. 1–5.
20. Tomczuk, B.; Weber, D. Effect of Magnetic Shunts on Shell-Type Transformers Characteristics. *Energies* **2023**, *16*, 6814. [[CrossRef](#)]
21. Kulkarni, S.V.; Khaparde, S.A. Stray losses in structural components. In *Transformer Engineering: Design and Practice*, 1st ed.; CRC Press: Boca Raton, FL, USA, 2004; pp. 169–230.
22. Hernandez, I.A.; Olivares-Galvan, J.C.; Georgilakis, P.S.; Canedo, J. Core loss and excitation current model for wound core distribution transformers. *Int. Trans. Electr. Energy Syst.* **2014**, *24*, 30–42. [[CrossRef](#)]
23. Kulan, M.C.; Baker, N.J.; Liogas, K.A.; Davis, O.; Taylor, J.; Korsunsky, A.M. Empirical Implementation of the Steinmetz Equation to Compute Eddy Current Loss in Soft Magnetic Composite Components. *IEEE Access* **2022**, *10*, 14610–14623. [[CrossRef](#)]
24. Chang, W.-C.; Kuo, C.-C.; Lin, W.-C.; Hsieh, M.-N. Simulation of Stray and Core Shielding Loss for Power Transformer Based on 2D/3D FEM. *IEEE Access* **2023**, *11*, 16943–16950. [[CrossRef](#)]
25. Zhu, Z.; Xie, D.; Wang, G.; Zhang, Y.; Yan, X. Computation of 3-D magnetic leakage field and stray losses in large power transformer. *IEEE Trans. Magn.* **2012**, *48*, 739–742. [[CrossRef](#)]
26. ABB Power Technologies Business Unit Transformers. *Transformer Handbook*; ABB Group: Zurich, Switzerland, 2004; pp. 146–149.
27. Thango, B.A.; Bokoro, P.N. Stray Load Loss Valuation in Electrical Transformers: A Review. *Energies* **2022**, *15*, 2333. [[CrossRef](#)]

**Disclaimer/Publisher’s Note:** The statements, opinions and data contained in all publications are solely those of the individual author(s) and contributor(s) and not of MDPI and/or the editor(s). MDPI and/or the editor(s) disclaim responsibility for any injury to people or property resulting from any ideas, methods, instructions or products referred to in the content.